A Sulfur-Tolerant MOF-Based Single-Atom Fe Catalyst for Efficient Oxidation of NO and Hg^0

Weijie Yang, Xiaoshuo Liu, Xuelu Chen, Yue Cao, Shaoping Cui, Long Jiao, Chongchong Wu, Chuanmin Chen, Dong Fu, Ian D. Gates, Zhengyang Gao,* and Hai-Long Jiang*

Catalytic oxidation of NO and Hg^0 is a crucial step to eliminate multiple pollutants from emissions from coal-fired power plants. However, traditional catalysts exhibit low catalytic activity and poor sulfur resistance due to low activation ability and poor adsorption selectivity. Herein, a single-atom Fe decorated N-doped carbon catalyst (Fe$_1$-N$_4$-C), with abundant Fe$_1$-N$_4$ sites, based on a Fe-doped metal–organic framework is developed to oxidize NO and Hg^0. The results demonstrate that the Fe$_1$-N$_4$-C has ultrahigh catalytic activity for oxidizing NO and Hg^0 at low and room temperature. More importantly, Fe$_1$-N$_4$-C exhibits robust sulfur resistance as it preferably adsorbs reactants over sulfur oxides, which has never been achieved before with traditional catalysts. Furthermore, SO$_2$ boosts the catalytic oxidation of NO over Fe$_1$-N$_4$-C through accelerating the circulation of active sites. Density functional theory calculations reveal that the Fe$_1$-N$_4$ active sites result in a low energy barrier and high adsorption selectivity, providing detailed molecular-level understanding for its excellent catalytic performance. This is the first report on NO and Hg^0 oxidation over single-atom catalysts with strong sulfur tolerance. The outcomes demonstrate that single-atom catalysts are promising candidates for catalytic oxidation of NO and Hg^0 enabling cleaner coal-fired power plant operations.

1. Introduction

Coal-fired power generation plays a crucial role in national economic development and energy security, especially in countries using coal as the main primary energy source.[1] Efficient removal of gaseous pollutants from coal-fired power plant remains a great challenge due to the conflicting redox environment demands of the different pollutants. Specifically, selective catalytic reduction (SCR) for denitrification undesirably inhibits the catalytic oxidation of elemental mercury (Hg^0).[2] To address this pressing issue, synergistic removal of multiple pollutants with a unified redox environment is highly expected.

Catalytic oxidation is a promising method for synergistic removal of multiple pollutants at low temperatures and in particular, is regarded as an ideal way to oxidize NO and Hg^0, after which the oxidation products (NO$_2$ and Hg^{2+}) can be simultaneously removed by alkaline solution.[3] Therefore, catalytic oxidation can simultaneously remove multiple pollutants without a complex process, which significantly improves the safety and economy of the coal-fired power plant. Although there are many advantages toward catalytic oxidation of NO and Hg^0 in coal-fired flue gas, there are still two main challenges: 1) currently used catalysts usually require high operation temperatures for NO oxidation while exhibiting low catalytic activity at moderate temperatures;[4] and 2) the active sites of catalysts are easily poisoned by SO$_2$ in flue gas, giving rise to significant deactivation.[5] Therefore, powerful catalysts featuring high activity at low temperatures and excellent SO$_2$ resistance are highly desired for the synergistic removal of multi-pollutants.

Single-atom catalysts (SACs), with the metal atoms atomically dispersed, can realize the maximized utilization and coordinative unsaturation of metal atoms.[6,7] The coordinatively unsaturated active sites of SACs usually possess unoccupied orbitals for oxygen activation which render them particularly promising in various oxidation reactions, such as the oxidation of methane and benzene at room temperature.[8] In addition, the uniform active sites in SACs make it possible to selectively adsorb specific reactants, endowing SACs with excellent antipoisoning properties.[9] Among the various strategies put forward for the construction of SACs, metal–organic frameworks (MOFs), with

W. Yang, X. Liu, X. Chen, Z. Gao
Department of Power Engineering
School of Energy
Power and Mechanical Engineering
North China Electric Power University
Baoding, Hebei 071003, P. R. China
E-mail: gaozhyan@163.com
Y. Cao, S. Cui, C. Chen, D. Fu
Department of Environmental Science and Engineering
North China Electric Power University
Baoding, Hebei 071003, P. R. China
L. Jiao, H.-L. Jiang
Hefei National Laboratory for Physical Sciences at the Microscale
Department of Chemistry
University of Science and Technology of China
Hefei, Anhui 230026, P. R. China
E-mail: jianglab@ustc.edu.cn
C. Wu, I. D. Gates
Department of Chemical and Petroleum Engineering
University of Calgary
Calgary, Alberta T2N 1C-N, Canada

**ADVANCED
SCIENCE NEWS**
www.advancedsciencenews.com

**ADVANCED
MATERIALS**
www.advmat.de
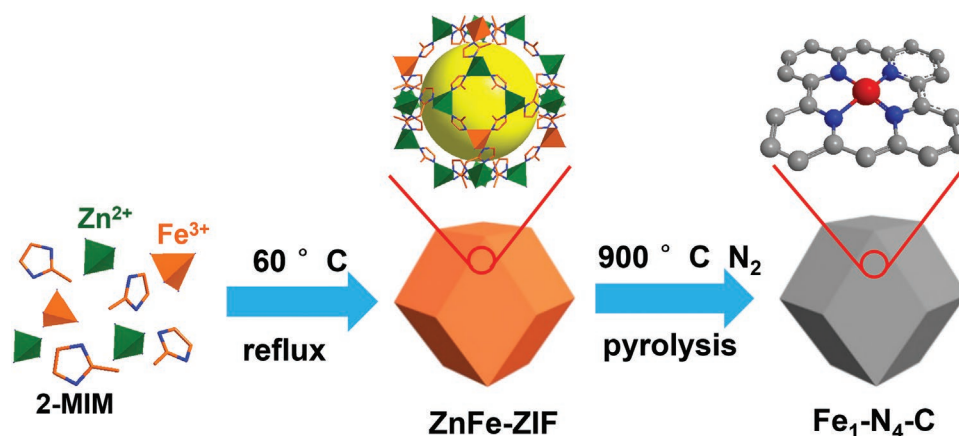
Scheme 1. Schematic illustration showing the fabrication strategy of Fe_1-N_4-C catalyst.

periodic structures, high porosity, and flexible tailorability, have shown great potential for the accurate construction and performance optimization of SACs.[10] Therefore, MOF-based SACs might be promising candidates to overcome the drawbacks of traditional catalysts in the catalytic oxidation of NO and Hg^0 from coal-fired flue gas.

In this work, a series of density functional theory (DFT) calculations are described on SACs with different local coordination microenvironments and the results reveal that Fe_1-N_4 sites are the most promising candidate for catalytic oxidation of NO and Hg^0. A representative MOF, namely ZIF-8 (also named as MAF-4), as selected for introducing Fe dopants, affording Fe-doped ZIF-8 as a precursor (**Scheme 1**).[11] Upon pyrolysis, single-atom Fe decorated N-doped carbon catalyst (denoted Fe_1-N_4-C), with abundant Fe-N_4 sites, is obtained which exhibits exceptionally high activity for the oxidation of NO and Hg^0. Strikingly, SO_2 is no longer a poisoning agent but rather enhances the catalytic oxidation of NO to some extent, which is completely different from the obvious deactivation as observed in previously reported catalysts.[12] To the best of our knowledge, this is the first report on SACs for the highly efficient catalytic oxidation of NO and Hg^0 with strong sulfur tolerance.

2. Results and Discussion

2.1. Theoretical Screening of SACs with Robust Reactivity and Selectivity

The adsorption behavior of reactants (NO, O_2, etc.) and sulfur oxides (SO_2 and SO_3) reflects the nature of active sites. The greater the adsorption energy of reactants superior to sulfur oxides, the higher selectivity of adsorption and stronger resistance of sulfur poisoning. Therefore, the adsorption energies of O_2, NO, SO_2, and SO_3 in flue gas have been first investigated by DFT calculation (details provided in Section S6, Supporting Information). As the catalytic behaviors of SACs are highly sensitive to the local coordination microenvironments such as coordination number and coordinated atoms,[13] four typical single-atom Fe sites (named as Fe_1-C_x or Fe_1-N_x, with x

representing the coordination number) have been constructed (**Figure 1**a–d). Adsorption behaviors of O_2, NO, SO_2, and SO_3 over four typical single-atom Fe sites have been investigated (Figure 1e and Figure S1, Supporting Information). It can be seen that the adsorption energies of reactants on these single-atom Fe sites are obviously different (Figure 1e). The O_2, NO, SO_2, and SO_3 present stable chemisorption on Fe_1-C_3, Fe_1-C_4, and Fe_1-N_3 active sites (Figure 1e), suggesting that SO_2 and SO_3 might occupy active sites of Fe_1-C_3, Fe_1-N_3, and Fe_1-C_4 leading to sulfur poisoning. Unexpectedly, the adsorption of SO_2 and SO_3 on Fe_1-N_4 sites is weak physical adsorption ($E_{ads} < -0.5$ eV), whereas the chemisorption for O_2 and NO remains well, manifesting that Fe_1-N_4 sites can preferentially adsorb NO and O_2 without sulfur poisoning (Figure 1e).

2.2. Synthesis and Characterization of Fe_1-N_4-C

Encouraged by the optimized adsorption selectivity of Fe_1-N_4 sites as indicated by the DFT calculations, Fe_1-N_4-C was synthesized. The Fe-doped zeolite imidazole framework-8 (denoted Fe-doped ZIF-8), featuring the same structure and morphology as ZIF-8, was constructed by using mixed metal ions (Zn^{2+} and Fe^{3+}) and 2-methylimidazole linker (**Figure 2**a; Figures S2a and S3, Supporting Information).[14] Upon pyrolysis at 900 °C under a N_2 atmosphere, the Fe_1-N_4-C catalyst was produced with ≈30 nm dimensions which was finer than the original MOF precursors (55 nm), as indicated by scanning electron microscope observation (Figure 2a,b). Transmission electron microscopy (TEM) and high-resolution TEM (HRTEM) images demonstrate the porous characteristic of Fe_1-N_4-C inherited from the MOF precursor and no Fe particles are observed (Figure 2c,d). Given the highly porous structure of Fe-doped ZIF-8 precursor, Fe_1-N_4-C exhibits considerable BET surface area up to 1249 m^2 g^{-1} (Figure S4, Supporting Information), favorable to the exposure of catalytic sites and the mass transfer process. Powder X-ray diffraction (XRD) pattern of Fe_1-N_4-C shows two broad peaks at ≈26° and ≈44°, respectively corresponding to the (002) and (101) reflections of graphitic carbon (Figure S2b, Supporting Information). No peak of Fe-based species can be detected, in
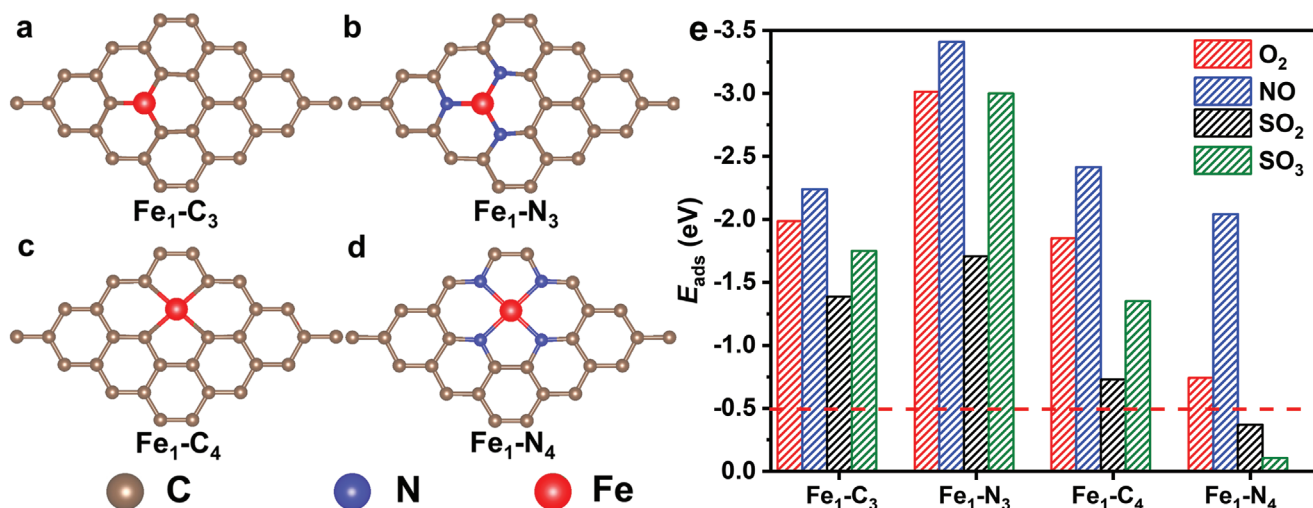
Figure 1. Geometric structures of single-atom Fe catalyst with four typical coordination environments including a) Fe$_1$-C$_3$, b) Fe$_1$-N$_3$, c) Fe$_1$-C$_4$, and d) Fe$_1$-N$_4$. e) The adsorption energies (E_{ads}) of O$_2$, NO, SO$_2$, and SO$_3$ over different single-atom Fe sites.

consistent with the TEM results (Figure 2c,d and Figure S2b, Supporting Information). The Raman spectrum of Fe$_1$-N$_4$-C presents a much lower intensity ratio of D band (1353 cm^{-1}) and G band (1590 cm^{-1}) than that of N-doped carbon (N-C) derived from ZIF-8, indicating that Fe doping is favorable to improve the graphitization degree of Fe$_1$-N$_4$-C (Figure S5, Supporting Information).

To investigate the chemical composition and existing state of Fe$_1$-N$_4$-C, X-ray photoelectron spectroscopy (XPS) was performed. The Fe 2p$_{3/2}$ peak is located at 710.8 eV, illustrating the oxidized state of Fe in Fe$_1$-N$_4$-C (Figure S6b, Supporting Information).[15] In addition, the N 1s spectrum can be fitted into five characteristic peaks and the peak centered at 399.2 eV proves the existence of Fe-N species in Fe$_1$-N$_4$-C (Figure S6a,
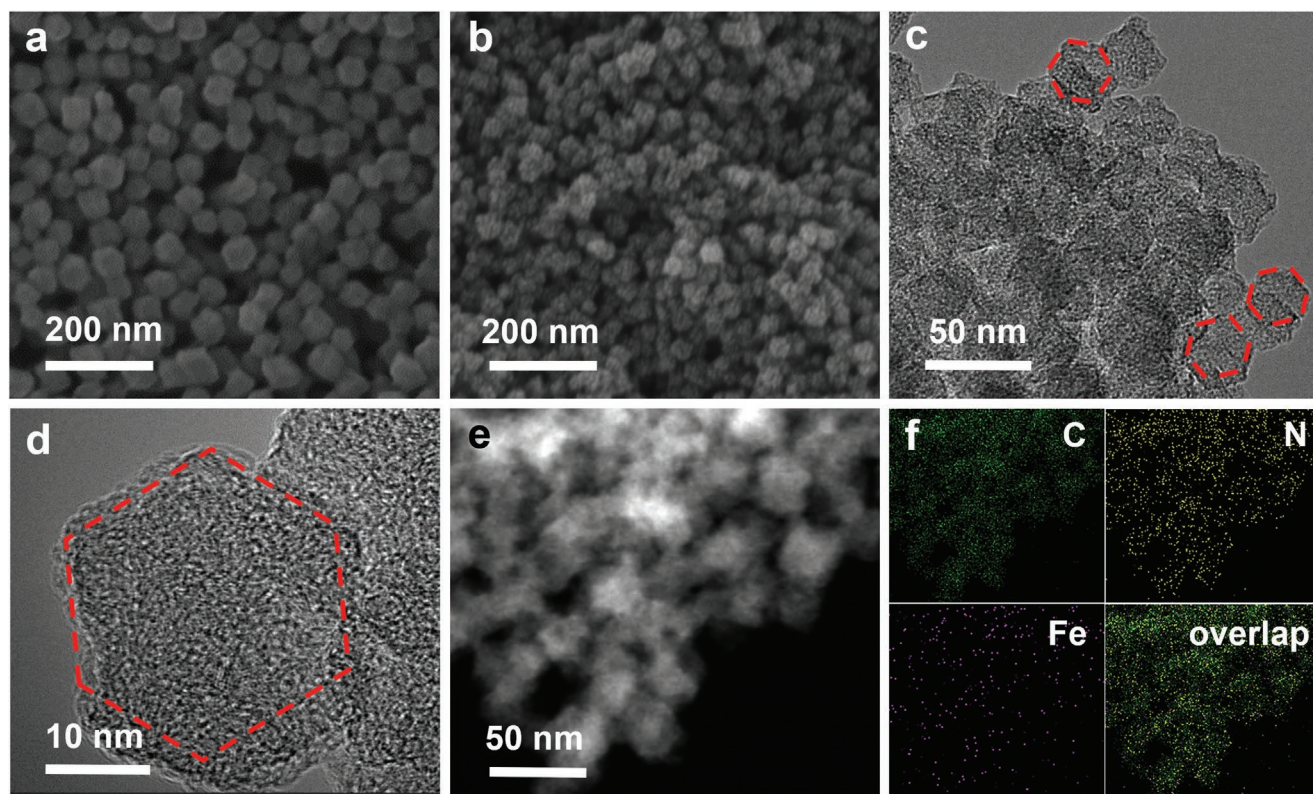

Figure 2. Scanning electron microscopy (SEM) images of a) Fe-doped ZIF-8 and b) Fe$_1$-N$_4$-C. c) TEM and d) HRTEM images of Fe$_1$-N$_4$-C. e) HAADF-STEM image and f) its corresponding elemental mapping for Fe$_1$-N$_4$-C.

**ADVANCED
SCIENCE NEWS**
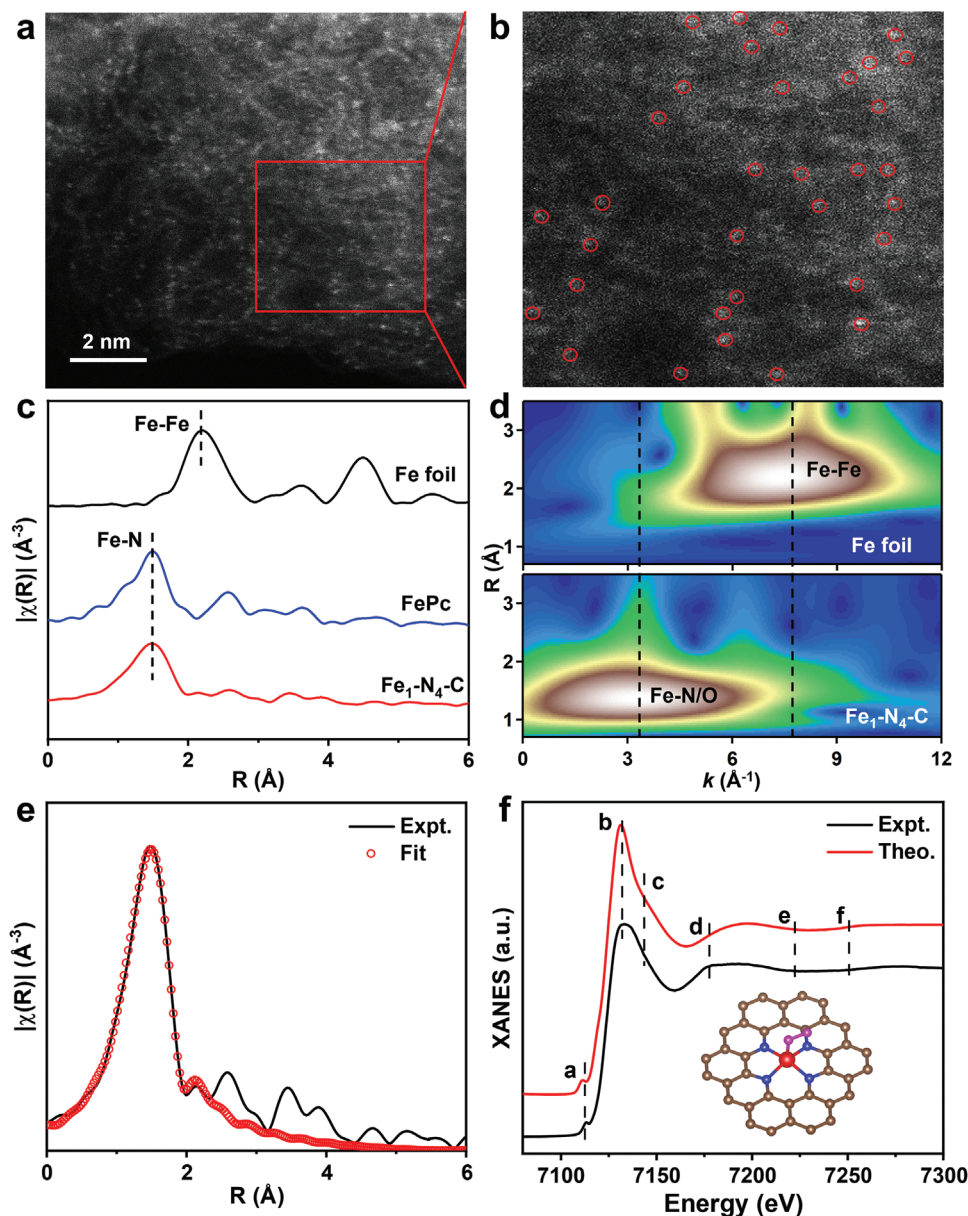
www.advancedsciencenews.com

**ADVANCED
MATERIALS**

www.advmat.de

Figure 3. a,b) Aberration-corrected HAADF-STEM images of Fe_1-N_4-C (single Fe atoms are highlighted by red circles). c) FT-EXAFS spectra of FePc, Fe foil, and Fe_1-N_4-C. d) EXAFS WT plots of Fe foil and Fe_1-N_4-C. e) EXAFS fitting for Fe_1-N_4-C. f) Comparison between the experimental K-edge XANES spectra of Fe_1-N_4-C and theoretical spectra calculated based on inset structural model (inset: structural model; Fe red, N blue, C brown, O pink).

Supporting Information).[16] Furthermore, single Fe atoms can be unambiguously identified in the aberration-corrected high-angle annular dark field scanning transmission electron microscope (HAADF-STEM) image of Fe_1-N_4-C where no Fe particles or clusters can be found (**Figure 3**a,b). Meanwhile, the elemental mapping image demonstrates the homogenous dispersion of Fe and N elements throughout the carbon matrix in Fe_1-N_4-C (Figure 2e,f). The results above clearly reveal the presence of atomic dispersion of Fe atoms in Fe_1-N_4-C. Furthermore, the content of Fe is also quantified to be 1.43 wt% using inductively coupled plasma atomic emission spectrometry (ICP-AES).

In addition to the characterizations for the local microstructural information above, the more powerful technique, X-ray

absorption spectroscopy (XAS), was used to determine electronic and structural information of Fe_1-N_4-C. According to the Fe K-edge X-ray absorption near-edge structure (XANES) spectra, the energy absorption threshold of Fe_1-N_4-C locates at a higher energy region than that of Fe foil, manifesting the positively charged $Fe^{\delta+}$ in Fe_1-N_4-C (Figure S7, Supporting Information), in line with the XPS results (Figure S6a, Supporting Information). The Fe K-edge Fourier transform-extended X-ray absorption fine structure (FT-EXAFS) spectra of Fe_1-N_4-C and iron phthalocyanine (FePc) show a dominant peak at ≈1.5 Å, corresponding to the Fe-N scattering path without Fe—Fe bond (≈2.2 Å) (Figure 3c). In addition, EXAFS wavelet transform (WT) plots strongly confirm that the atomic dispersion of Fe
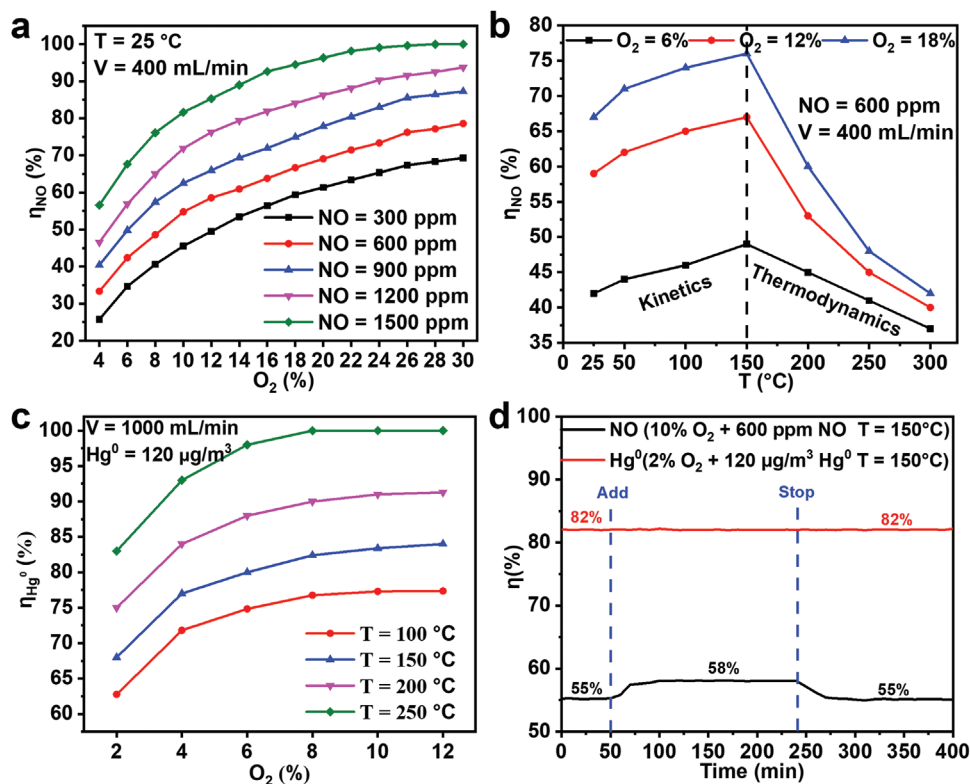
Figure 4. a) The NO oxidation rates of Fe$_1$-N$_4$-C at different concentrations of NO and O$_2$ at 25 °C. b) The NO oxidation rates of Fe$_1$-N$_4$-C at different temperatures and O$_2$ concentrations. c) Hg^0 oxidation rates of Fe$_1$-N$_4$-C at different temperatures and O$_2$ concentrations. d) Catalytic oxidation rates of NO and Hg^0 over Fe$_1$-N$_4$-C with the addition of 500 ppm SO$_2$.

in Fe$_1$-N$_4$-C is similar to FePc (Figure 3d and Figure S8, Supporting Information). The best-fitting analysis for the EXAFS spectrum of Fe$_1$-N$_4$-C shows that Fe atom is coordinated by four N atoms and one O atom (Figure 3e and Table S1, Supporting Information). XANES simulation has been carried out to further confirm the coordination configurations of Fe in Fe$_1$-N$_4$-C (Figure 3f). After a series of optimizations, planar configurational Fe$_1$-N$_4$ moiety coordinated with an axial oxygen atom from O$_2$, illustrates the most consistent K-edge XANES spectrum with the experimental data (Figure 3f).[17] The obtained structure based on XANES simulation suggests that the test sample adsorbs oxygen molecular after exposure to air environment and is also self-consistent to the structure of O$_2$ adsorption on Fe$_1$-N$_4$ site from the DFT calculation above (Figure 3f and Figure S1, Supporting Information).

2.3. Catalytic Conversion of NO and Hg^0 on Fe$_1$-N$_4$-C

2.3.1. Catalytic Performance Assessment

With the DFT and experimental results above, the Fe$_1$-N$_4$ sites have been successfully constructed in Fe$_1$-N$_4$-C. Inspired by this, the catalytic performance of Fe$_1$-N$_4$-C for oxidation of NO and Hg^0 has been separately evaluated in a fixed-bed flow reactor (Figure S9, Supporting Information). The results, plotted in **Figure 4**, show that the Fe$_1$-N$_4$-C catalyst exhibits excellent activity toward NO oxidation even at room temperature,

far surpassing traditional metal oxide catalysts which usually show activity at temperatures higher than 200 °C.[18] This demonstrates the huge potential of Fe$_1$-N$_4$-C for oxidation of NO at moderate and low temperatures. By varying the concentrations of NO and O$_2$ at 25 °C, the oxidation rate of NO (η_{NO}) grows gradually with the increased concentrations of O$_2$ and NO and reaches 100% at 1500 ppm NO and 26% O$_2$ (Figure 4a). The catalytic activity of Fe$_1$-N$_4$-C under elevated temperatures has been further examined. As shown in Figure 4b, as the temperatures rises from 25 to 300 °C, η_{NO} firstly rises before 150 °C and then decreases beyond, presenting a volcano profile mainly due to the competition between the energy barrier in kinetics and reaction thermodynamic equilibrium.[18] Specifically, as the temperature increases from 25 to 150 °C, molecular activation is promoted under reaction equilibrium leading to increased η_{NO} at higher temperatures. However, when the temperature exceeds 150 °C, the reverse reaction is faster competing with the promotion of molecular activation resulting in the decrease of η_{NO} when the temperature rises further. Interestingly, when the temperature falls from 300 to 150 °C, η_{NO} recovers to the original value exhibited at 150 °C, unambiguously providing evidence that deactivation of Fe$_1$-N$_4$-C at such high temperature does not occur (Figure S11, Supporting Information).

In addition to NO oxidation, the catalytic oxidation of Hg^0 has also been investigated versus temperatures and O$_2$ concentrations. The η_{Hg}^0 reaches 100% at 8% O$_2$ concentration and 250 °C, illustrating the superior catalytic performance of Fe$_1$-N$_4$-C for Hg^0 oxidation (Figure 4c). Compared with activated
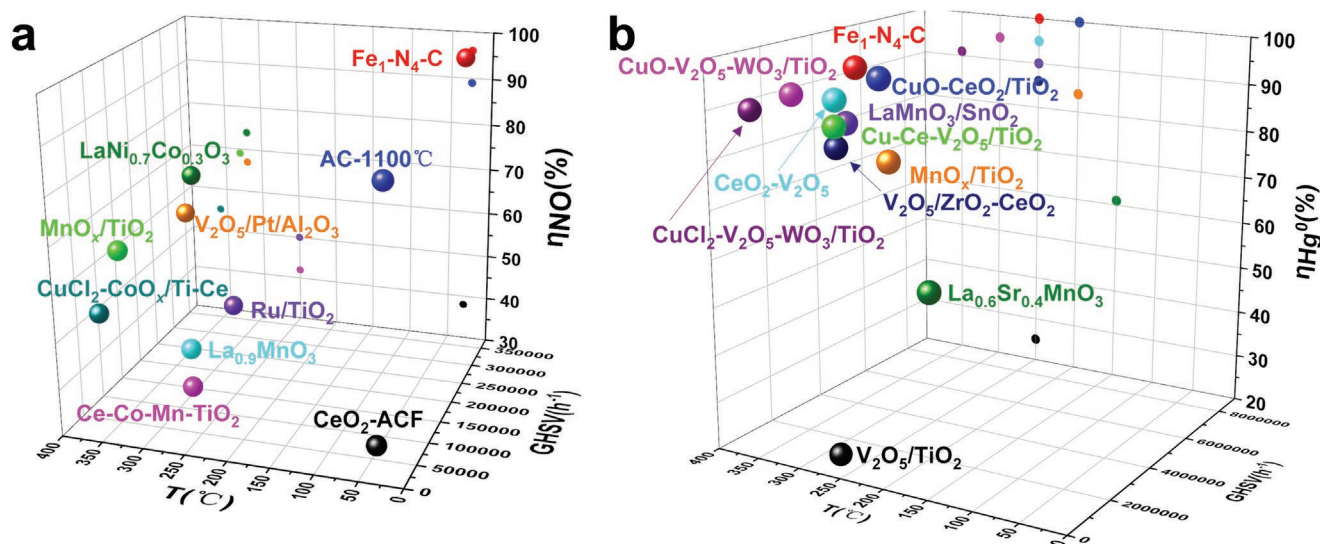
Figure 5. Comparison of the catalytic performance between Fe_1-N_4-C and other catalysts on catalytic oxidation of a) NO (Raw data from Table S3, Supporting Information) and b) Hg^0 (Raw data from Table S4, Supporting Information).

carbon and metal oxide catalysts, Fe_1-N_4-C has higher efficiency for the oxidation of NO and Hg^0 at a larger space velocity and lower temperature, testifying to its superior catalytic activity of Fe_1-N_4-C over that of traditional catalysts (Tables S2 and S3, Supporting Information, and **Figure 5**).[19] In detail, Fe_1-$N4$-C achieves 100% η_{Hg}^0 at a gas hourly space velocity (GHSV) of 8.5×10^5 h^{-1}, which is 20 times larger than commercial SCR catalysts, such as V_2O_5/TiO_2 (Table S3, Supporting Information).

2.3.2. Sulfur-Tolerant Assessment

Given that SO_2 in flue gas is one of the main factors that causes poisoning and deactivation of catalysts,[20] catalytic oxidations of NO and Hg^0 have been investigated in the existence of SO_2. Surprisingly, the η_{Hg}^0 can be well maintained in the presence of 500 ppm SO_2, as shown in Figure 4d, indicating negligible influence of SO_2 on the activity of Fe_1-N_4-C. To our knowledge, this is the first catalyst for Hg^0 oxidation that does not get poisoned under such a high concentration of SO_2, which is distinctly different from the severe deactivation of other reported catalysts (Table S5, Supporting Information).[21] The weak physical adsorption of SO_2 and SO_3 and stable chemisorption of reactants on Fe_1-N_4-C, as demonstrated by the DFT calculation above (Figure 1e), should be responsible for this robust sulfur resistance, which is of critical importance in coal-fired power plants. Moreover, the sulfur resistance of Fe_1-N_4-C during NO oxidation has also been tested (Figure 4d). Strikingly, opposite to the commonly observed deactivation in previous reports,[12] the introduction of SO_2 enhances the activity of Fe_1-N_4-C toward NO oxidation (≈3%) (Figure 4d and Table S4, Supporting Information). Once SO_2 introduction is stopped, the activity enhancement disappears immediately, returning to the original value before the introduction of SO_2 (Figure 4d). In the tail gas, about 1.1% SO_2 is oxidized into SO_3 (Figure S12, Supporting Information), indicating that the SO_2 participates in the catalytic oxidation reaction on Fe_1-N_4-C (Section S5,

Supporting Information). Therefore, in the presence of Fe_1-N_4-C catalyst, SO_2 molecules accelerate some reaction steps in NO oxidation rather than poison it as commonly observed with other catalysts. In addition, Fe_1-N_4-C displays stable oxidation rates of NO and Hg^0 after 60-hour long experiments (Figure S13, Supporting Information). The experimental results above clearly demonstrate the high catalytic activity, robust sulfur resistance and great stability of Fe_1-N_4-C for catalytic oxidations of NO and Hg^0, manifesting its particular advantages and great potential toward the synergistic removal of multiple pollutants in coal-fired power plants.

2.3.3. Molecular-Level Insight of Superior Catalytic Performance

To unveil the mechanism behind the high catalytic activity, robust sulfur resistance and high stability of Fe_1-N_4-C, DFT calculations have been further carried out to investigate energy variation along the reaction paths of NO and Hg^0 oxidation over Fe_1-N_4 sites (**Figure 6**a,b). For NO oxidation, the rate-determining step (RDS) correlates to the desorption of the second NO_2, with an energy barrier (E_b) of 1.26 eV. The energy barriers for the first and second NO_2 formation are only 0.01 and 0.42 eV, respectively (Figure 6a). Those low energy barriers of NO oxidation on Fe_1-N_4 sites account for the high NO conversion of Fe_1-N_4-C at low temperature, supporting the outstanding activity of Fe_1-N_4-C in the NO catalytic oxidation (Figure 4a). For Hg^0 oxidation, the RDS is the desorption of the second $(HgO)_2$ with an energy barrier of 2.34 eV, which is much lower than that of commercial SCR V_2O_5/TiO_2 (5.43 eV)[22] and ZnO (3.40 eV)[23] (Figure 6b). Consequently, Fe_1-N_4-C achieves 100% conversion of Hg^0 at higher GHSV than commercial SCR catalysts, which can be readily approved by its lower energy barrier of Hg^0 oxidation on Fe_1-N_4 sites. Compared with N-doped carbon (N-C), Fe_1-N_4 site can effectively adsorb and activate O_2 molecule through significant electron transfer between single-atom Fe and O_2 molecule (Figure S14, Supporting Information).
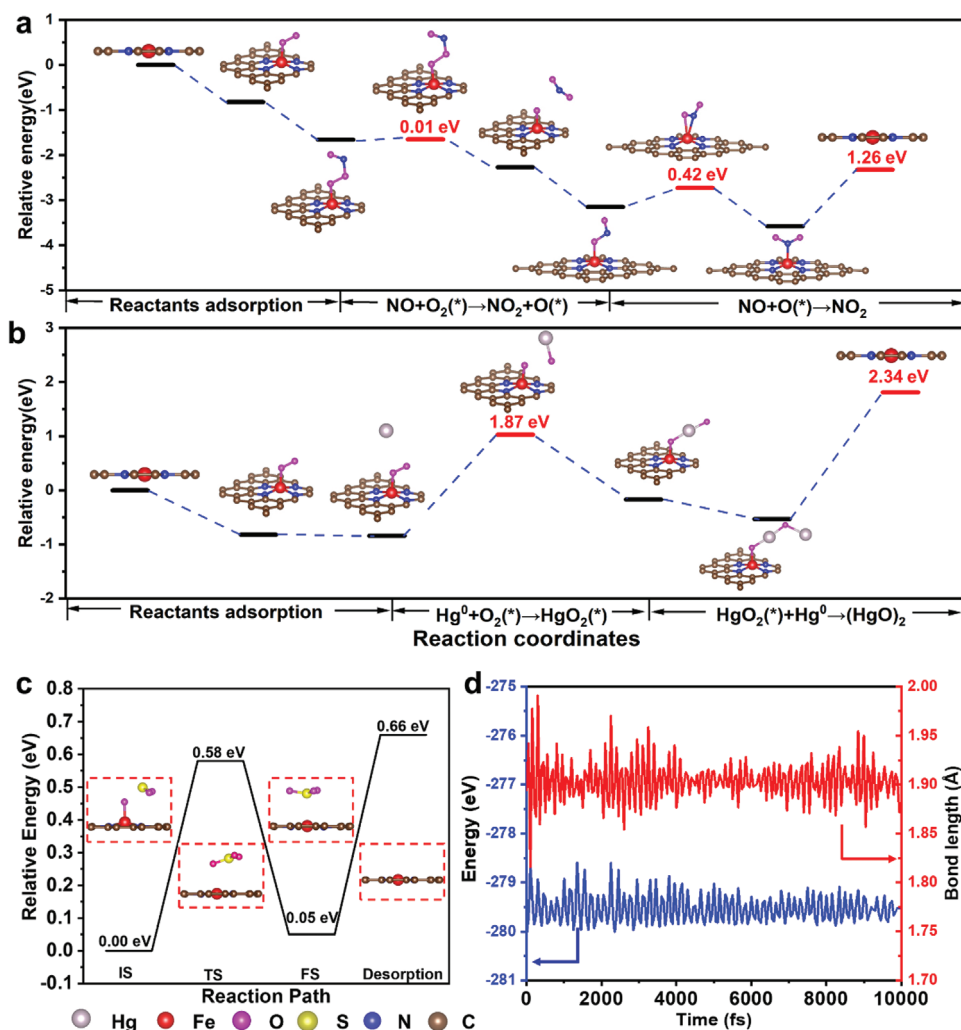
Figure 6. The energy variations along reaction path of a) NO and b) Hg^0 oxidation. c) Oxidation path between SO_2 and adsorbed O atom. d) Energy variation and average Fe—N bond length of Fe_1-N_4 sites in a 10000 fs AIMD simulation at the temperature of 500 °C.

Therefore, the superhigh catalytic activity of Fe_1-N_4-C at low temperature originates from the high activation ability of Fe_1-N_4 site for O_2 molecules.

As for the unprecedented activity enhancement effect of SO_2 for NO oxidation, the oxidation path between SO_2 and adsorbed O atom has been investigated by DFT calculations (Figure 6c). The results show that SO_2 can be easily oxidized by the adsorbed O atom on Fe_1-N_4 sites with a low energy barrier of 0.58 eV. The RDS is the desorption of SO_3, with an energy barrier of 0.61 eV, which is obviously lower than that of second NO oxidation (1.26 eV) (Figure 6a). Therefore, we believe that the addition of SO_2 accelerates the consumption of residual O atoms on Fe_1-N_4 sites, thereby boosting the catalytic cycle of NO oxidation.

To further understand the structural stability of Fe_1-N_4, ab initio molecular dynamics (AIMD) simulation was conducted at 500 °C for a relatively long time duration (10 000 fs). The variations of energy and average Fe—N bond length fluctuate in the ranges of −280 to −279 eV and 1.85 to 1.95 Å, respectively (Figure 6d). The results suggest that Fe_1-N_4-C can keep

the coordination structure of Fe_1-N_4 even at such a high temperature, in good agreement with the high stability of Fe_1-N_4-C observed in the experiments.

3. Conclusions

A single-atom Fe catalyst, Fe_1-N_4-C with abundant coordinatively unsaturated Fe_1-N_4 sites, was fabricated from Fe-doped ZIF-8 precursor followed by controlled pyrolysis. The unique Fe_1-N_4 sites in Fe_1-N_4-C enable the direct conversion of NO to NO_2 even at room temperature. Meanwhile, $Hg°$ can also be oxidized by Fe_1-N_4-C with ultrahigh gas hourly space velocity. Strikingly, Fe_1-N_4-C affords robust catalytic stability against sulfur poisoning, which has never been observed thus far. DFT calculations reveal that the moderate energy barriers are responsible for the efficient oxidation of NO and Hg^0 at relatively low temperatures. The robust sulfur resistance of Fe_1-N_4-C originates from the preferable adsorption of reactants rather than SO_2 and SO_3 on Fe_1-N_4 sites. Moreover, the

unprecedented activity enhancement effect of SO_2 toward NO oxidation is ascribed to the accelerated consumption of adsorbed O atoms on Fe_1-N_4 sites promoted by SO_2 oxidation, leading to the regeneration of Fe_1-N_4 sites. This work not only develops exceptionally efficient and unprecedented sulfur-resistant SACs but also provides new insights toward catalytic oxidation of NO and Hg^0 for the removal of multiple pollutants in coal-fired power plants.

Supporting Information

Supporting Information is available from the Wiley Online Library or from the author.

Conflict of Interest

The authors declare no conflict of interest.

Data Availability Statement

The data that support the findings of this study are available from the corresponding author upon reasonable request.

Keywords

catalytic oxidation, heterogeneous catalysis, metal–organic frameworks, single-atom catalysis

[1] L. Bernard, BP Statistical Review of World Energy, *British Petroleum Corporate Communications Services*, London, UK **2021**, p. 2021.

[2] S. Zhao, D. Pudasainee, Y. Duan, R. Gupta, M. Liu, J. Lu, *Prog. Energy Combust. Sci.* **2020**, *73*, 26.

[3] a) L. Ma, W. Zhang, Y.-G. Wang, X. Chen, W. Yu, K. Sun, H. Sun, J. Li, J. W. Schwank, *Appl. Catal., B* **2020**, *267*, 118371; b) Z. Wang, J. Liu, B. Zhang, Y. Yang, Z. Zhang, S. Miao, *Environ. Sci. Technol.* **2016**, *50*, 5398; c) J. Li, H. Xu, Z. Huang, Q. Huang, Y. Qiu, N. Yan, Z. Qu, *Environ. Sci. Technol.* **2021**, *55*, 14126; d) T. Jia, J. Wu, Z. Ji, C. Peng, Q. Liu, M. Shi, J. Zhu, H. Wang, D. Liu, M. Zhou, *Appl. Catal., B* **2021**, *284*, 119727; e) X. Zhang, X. Han, Y. Wei, X. Wang, N. Zhang, J. Bao, H. He, *Chem. Eng. J.* **2022**, *428*, 132660; f) Y. Zhang, Y. Zhao, Z. Zhou, T. Gao, B. Gong, P. Liu, J. Liu, J. Zhang, *Appl. Catal., B* **2021**, 119534.

[4] L. Li, L. Qu, J. Cheng, J. Li, Z. Hao, *Appl. Catal., B* **2009**, *88*, 224.

[5] K. Wijayanti, K. Xie, A. Kumar, K. Kamasamudram, L. Olsson, *Appl. Catal., B* **2017**, *216*, 142.

[6] a) B. Qiao, A. Wang, X. Yang, L. F. Allard, Z. Jiang, Y. Cui, J. Liu, J. Li, T. Zhang, *Nat. Chem.* **2011**, *3*, 634; b) A. Wang, J. Li, T. Zhang, *Nat. Rev. Chem.* **2018**, *2*, 65; c) C. Jia, X. Tan, Y. Zhao, W. H. Ren, Y. B. Li, Z. Su, S. C. Smith, C. Zhao, *Angew. Chem., Int. Ed.* **2021**, *60*, 23342; d) X. Wang, Y. Jia, X. Mao, D. Liu, W. He, J. Li, J. Liu, X. Yan, J. Chen, L. Song, A. Du, X. Yao, *Adv. Mater.* **2020**, *32*, 2000966; e) C. Tang, Y. Jiao, B. Shi, J.-N. Liu, Z. Xie, X. Chen, Q. Zhang, S.-Z. Qiao, *Angew. Chem., Int. Ed.* **2020**, *59*, 9171; f) C.-C. Hou, H.-F. Wang, C. Li, Q. Xu, *Energy Environ. Sci.* **2020**, *13*, 1658.

[7] a) W. Guo, Z. Wang, X. Wang, Y. Wu, *Adv. Mater.* **2021**, *33*, 2004287; b) Y. Liu, X. Wu, Z. Li, J. Zhang, S.-X. Liu, S. Liu, L. Gu, L. Zheng, J. Li, D. Wang, Y. Li, *Nat. Commun.* **2021**, *12*, 4205; c) L. Liu, A. Corma, *Chem. Rev.* **2018**, *118*, 4981; d) H. Zhang, P. An, W. Zhou, B. Y. Guan, P. Zhang, J. Dong, X. W. Lou, *Sci. Adv.* **2018**, *4*, eaao6657; e) S. H. Talib, Z. Lu, X. Yu, K. Ahmad, B. Bashir, Z. X. Yang, J. Li, *ACS Catal.* **2021**, *11*, 8929.

[8] a) D. Deng, X. Chen, L. Yu, X. Wu, Q. Liu, Y. Liu, H. Yang, H. Tian, Y. Hu, P. Du, R. Si, J. Wang, X. Cui, H. Li, X. Jiao, T. Xu, J. Deng, F. Yang, P. N. Duchesne, P. Zhang, J. Zhou, L. Sun, J. Li, X. Pan, X. Bao, *Sci. Adv.* **2015**, *1*, e1500462; b) X. Cui, H. Li, Y. Wang, Y. Hu, L. Hua, H. Li, X. Han, Q. Liu, F. Yang, L. He, Q. Chen, Q. Li, J. Xiao, H. Deng, X. Bao, *Chem* **2018**, *4*, 1902.

[9] a) J. Liu, F. R. Lucci, M. Yang, S. Lee, M. D. Marcinkowski, A. J. Therrien, C. T. Williams, E. C. H. Sykes, M. Flytzani-Stephanopoulos, *J. Am. Chem. Soc.* **2016**, *138*, 6396; b) A. K. Datye, M. Votsmeier, *Nat. Mater.* **2021**, *20*, 1049; c) Y. Pan, Y. Chen, K. Wu, Z. Chen, S. Liu, X. Cao, W.-C. Cheong, T. Meng, J. Luo, L. Zheng, C. Liu, D. Wang, Q. Peng, J. Li, C. Chen, *Nat. Commun.* **2019**, *10*, 4290.

[10] a) J. Wang, Z. Li, Y. Wu, Y. Li, *Adv. Mater.* **2018**, *30*, 1801649; b) L. Jiao, H.-L. Jiang, *Chem* **2019**, *5*, 786; c) H. Furukawa, K. E. Cordova, M. O'Keeffe, O. M. Yaghi, *Science* **2013**, *341*, 1230444; d) J.-S. Qin, S. Yuan, L. Zhang, B. Li, D.-Y. Du, N. Huang, W. Guan, H. F. Drake, J. Pang, Y.-Q. Lan, A. Ali, H.-C. Zhou, *J. Am. Chem. Soc.* **2019**, *141*, 2054.

[11] a) K. S. Park, Z. Ni, A. P. Côté, J. Y. Choi, R. Huang, F. J. Uribe-Romo, H. K. Chae, M. O'Keeffe, O. M. Yaghi, *Proc. Natl. Acad. Sci. USA* **2006**, *103*, 10186; b) X.-C. Huang, Y.-Y. Lin, J.-P. Zhang, X.-M. Chen, *Angew. Chem., Int. Ed.* **2006**, *45*, 1557; c) E. Proietti, F. Jaouen, M. Lefèvre, N. Larouche, J. Tian, J. Herranz, J.-P. Dodelet, *Nat. Commun.* **2011**, *2*, 416.

[12] a) H. Wang, H. Chen, Y. Wang, Y.-K. Lyu, *Chem. Eng. J.* **2019**, *361*, 1161; b) G. Li, Q. Wu, S. Wang, J. Li, X. You, S. Shao, M. Wen, L. Xu, Y. Tang, F. Wang, Y. Wang, K. Liu, *Environ. Sci. Technol.* **2019**, *54*, 1889.

[13] a) W. Yang, S. Xu, K. Ma, C. Wu, I. D. Gates, X. Ding, W. Meng, Z. Gao, *Nano Mater. Sci.* **2020**, *2*, 120; b) C. Chen, W. Ou, K. M. Yam, S. Xi, X. Zhao, S. Chen, J. Li, P. Lyu, L. Ma, Y. Du, W. Yu, H. Fang, C. Yao, X. Hai, H. Xu, M. J. Koh, S. J. Pennycook, J. Lu, M. Lin, C. Su, C. Zhang, J. Lu, *Adv. Mater.* **2021**, *33*, 2008471; c) Y. Sun, L. Silvioli, N. R. Sahraie, W. Ju, J. Li, A. Zitolo, S. Li, A. Bagger, L. Arnarson, X. Wang, T. Moeller, D. Bernsmeier, J. Rossmeisl, F. Jaouen, P. Strasser, *J. Am. Chem. Soc.* **2019**, *141*, 12372.

[14] H. Zhang, S. Hwang, M. Wang, Z. Feng, S. Karakalos, L. Luo, Z. Qiao, X. Xie, C. Wang, D. Su, Y. Shao, G. Wu, *J. Am. Chem. Soc.* **2017**, *139*, 14143.

[15] a) L. Jiao, G. Wan, R. Zhang, H. Zhou, S.-H. Yu, H.-L. Jiang, *Angew. Chem., Int. Ed.* **2020**, *132*, 20770; b) R. Zhang, L. Jiao, W. Yang, G. Wan, H.-L. Jiang, *J. Mater. Chem. A* **2019**, *7*, 26371.

[16] L. Jiao, R. Zhang, G. Wan, W. Yang, X. Wan, H. Zhou, J. Shui, S. Yu, H. L. Jiang, *Nat. Commun.* **2020**, *11*, 2831.

[17] H. Fei, J. Dong, Y. Feng, C. S. Allen, C. Wan, B. Volosskiy, M. Li, Z. Zhao, Y. Wang, H. Sun, P. An, W. Chen, Z. Guo, C. Lee, D. Chen, I. Shakir, M. Liu, T. Hu, Y. Li, A. I. Kirkland, X. Duan, Y. Huang, *Nat. Catal.* **2018**, *1*, 63.

[18] Z. Hong, Z. Wang, X. B. Li, *Catal. Sci. Technol.* **2017**, *7*, 3440.

[19] L. Zhao, C. Li, S. Li, Y. Wang, J. Zhang, T. Wang, G. Zeng, *Appl. Catal., B* **2016**, *198*, 420.

[20] Z. Ma, L. Sheng, X. Wang, W. Yuan, S. Chen, W. Xue, G. Han, Z. Zhang, H. Yang, Y. Lu, Y. Wang, *Adv. Mater.* **2019**, *31*, 1903719.

[21] a) Z. Zhou, L. Liu, X. Liu, Y. Zhou, C. Wang, J. Xu, G. Chang, M. Xu, *Fuel* **2022**, *310*, 122317; b) W. Chen, Y. Pei, W. Huang, Z. Qu, X. Hu, N. Yan, *Environ. Sci. Technol.* **2016**, *50*, 2564.

[22] Y. Gao, Z. Li, Y. Hao, *J. Phys. Chem. C* **2017**, *121*, 27963.

[23] L. Ling, S. Zhao, P. Han, B. Wang, R. Zhang, M. Fan, *Chem. Eng. J.* **2014**, *244*, 364.

2110123 (9 of 9)